ISSN 0016-7932, Geomagnetism and Aeronomy, 2020, Vol. 60, No. 8, pp. 1093–1100. © Pleiades Publishing, Ltd., 2020.

Sunspot Activity and Coronal Holes during the Declining Phase of Cycle 24

O. A. Andreeva[a], * and V. M. Malashchuk[a]

[a] *Crimean Astrophysical Observatory, Russian Academy of Sciences, Crimea, Russia*

**e-mail: olga@craocrimea.ru*

Received March 4, 2020; revised May 28, 2020; accepted May 29, 2020

Abstract—The dynamics of coronal holes (CHs) during the declining phase of solar cycle 24 is studied based on observational data from the Atmospheric Imaging Assembly (AIA), the 19.3 nm channel, of the Solar Dynamic Observatory (SDO). Some features of changes in the areas of polar and mid- and low-latitude CHs in the period April 1, 2014–December 31, 2019, are revealed by a comparison of the variations in the daily total CH area with the index of the sunspot number. The division of all CHs observed in the considered period into polar and nonpolar shows that polar-CH areas dominate and increase while nonpolar-CH areas constantly decrease toward the cycle minimum. Polar-CH areas account for ~80% of the total area of all CHs considered over the studied period. The total polar-CH area increases toward cycle minimum, which is consistent with the general concept of polar CHs as the main source of the Sun's dipole magnetic field. However, the second subset, which contains selected isolated CHs, shows an interesting behavior in the declining phase of solar activity that was not previously observed. Their areas slowly decrease from the maximum to minimum of the solar cycle. This trend is qualitatively consistent with a decrease in sunspot activity toward the minimum, which suggests a physical relationship between the two phenomena.

DOI: 10.1134/S0016793220080022

1. INTRODUCTION

The occurrence and cyclic evolution of coronal holes (CHs) depend on their relation to both the large-scale magnetic field and active regions (ARs). Coronal holes in ARs are related to the processes occurring in these regions, in particular, flares and coronal mass ejections. Coronal holes that are not related to ARs reflect the distribution of large-scale solar magnetic fields, and their dynamics is determined by global changes in the structure of the magnetic field of the Sun (Bilenko, 2004). A close relationship between CHs and ARs was found earlier (Levin, 1977; Bohlin and Sheeley, 1978; Sheeley and Harvey, 1981; Levin et al., 1977) and later confirmed (Obridko and Shelting, 2013, 2015; Malashchuk et al., 2012).

The role of ARs in the generation and subsequent evolution of CHs is beyond doubt. Nevertheless, the mechanism of the generation and evolution of polar and mid- and low-latitude CHs is not fully understood.

In the standard solar dynamo model (e.g., Hoyng, 1993), the initially dipole poloidal field in the solar minimum is wound by differential rotation into a strong toroidal field in the solar maximum. The polar CHs that dominate during the minimum are related to the poloidal field, while the higher sunspot number during the maximum is related to the toroidal field. The relationship between these two manifestations of the magnetic evolution of the Sun was first studied by Bravo and Otaola (1989). Later, Bravo and Stewart (1994, 1997) showed that there is a close relationship between the evolution of polar-CH areas estimated from K-coronameter observations and the sunspot number with a delay of about half of the solar cycle. Bravo and Stewart (1997) showed that the total area of CHs of all types is maximal in the minimum phase.

During the solar minimum, the regions of an open field over the poles (polar CHs) reach the maximum extension, and the number of low-latitude regions of the closed and strong field (active regions and sunspots) is minimal. As the cycle evolves, more sunspots appear and the polar CHs become smaller. Small, low-latitude CHs appear at this time, but the total area of the Sun covered by CHs decreases as the sunspot number increases.

During the declining phase of cycle 24, there were two pronounced intervals of dominant sunspot activity: first, in the southern (S) and then in the northern (N) hemispheres. The purpose of this article is to study the CH dynamics and to identify features of the changes in the polar and isolated CH areas in this cycle phase.

2. OBSERVATIONAL DATA, METHODS, AND STATISTICAL ANALYSIS

This article explores the temporal variations of the daily total CH area (daily total coronal hole area, S_{CH})

Table 1. Statistical analysis of coronal holes detected in the period Apr. 1, 2014–Dec. 31, 2019

Year	2014	2015	2016	2017	2018	2019	Total
Days	275	365	357	365	365	365	2092
CHs N-hem	722	887	887	806	740	577	4619
CHs S-hem	800	855	707	685	628	597	4272
CHs N_S_eq	82	174	96	106	78	17	553
CHs N_pol	221	251	411	452	485	495	2315
CHs S_pol	246	397	364	425	437	506	2375
CHs N_isol	501	636	476	354	255	82	2304
CHs S_isol	554	458	343	260	191	91	1897
All CHs	1522	1742	1594	1491	1368	1174	8891

The table contains statistical data on the processing of CHs in the period Apr. 1, 2014–Dec. 31, 2019. The top row (Year) lists the years of the studied period. The second row (Days) shows the number of days of CH observations analyzed in each year. Below is the annual information on the number of CHs for the N (CHs N-hem) and S (CHs S-hem) hemispheres, as well as on the number of CHs crossing the equator (CHs N_S_eq). The following table rows contain annual statistics on the number of polar (CHs N_pol, CHs S_pol) and isolated CHs (CHs N_isol, CHs S_isol) for the N and S hemispheres, respectively. The bottom row (All CHs) shows the annual total number of CHs detected on the entire visible surface of the Sun. The right column (Total) represents the total number of values corresponding to each row for the entire studied period.

during the declining phase of cycle 24. The study is based on observational data from the SDO/AIA instrument in the iron line (Fe XII 19.3 nm), from April 2014 to December 2019.

The solar corona is the source of very dynamic events that mainly take place in ARs and CHs. The exact location of these large-scale objects can be determined with the application of image-processing techniques to extreme ultraviolet (EUV) data. We used the Heliophysics Event Knowledgebase (HEK) (Hurlburt et al., 2012), which is available at http://www.lmsal.com/hek/hek_isolsearch.html, to locate CHs and determine their areas. Information on CHs was extracted with the spatial possibilistic clustering algorithm (SPoCA), which was described in detail by Barra et al. (2009) and Verbeeck et al. (2014). The SPoCA is a set of multichannel, fuzzy, clustering algorithms that automatically segment EUV solar images into a set of functions. The SPoCA separates ARs, quiet Sun, and CHs by minimizing fuzzy intraclass variance. It segments up to 0.99 $R_\odot$, excluding off-disk structures. These databases made it possible to obtain an array of daily total CH areas for the period April 1, 2014–December 31, 2019. The unit of measurement of the CH area is Mm^2.

In the course of the study, we processed more than 5.5 years (2092 days) of CH observations. During this period, we analyzed 8891 CHs, 553 of which crossed the equator. In our work, we assumed that the area of the CHs crossing the equator is divided into two parts, and each part belongs to the corresponding hemisphere, depending on its location. Taking this into account, 4619 CHs were detected in the N hemisphere and 4272 CHs were found in the S hemisphere. Table 1 shows that the statistical volume of the presented material is quite extensive and gives grounds for the study of the dynamics of different types of CHs during the cycle.

We used the sunspot index, SN, as an index of solar activity to analyze our material. It is generally accepted that the solar-activity index SN reflects an 11-year solar cyclicity and is therefore related to the solar dynamo. Conversely, the studied CHs are open-flux regions that are also generated by the solar dynamo. Therefore, it is expedient to compare the SN with the parameters of cyclic CH variations, in particular, their area. The daily total SN for the N and S hemispheres were taken from the Royal Belgian Observatory website (http://sidc.oma.be/silso/datafiles#hemi). We call the data divided by hemispheres the northern and southern components.

In our work, we also analyzed

—The smoothed total values of the monthly SN and S_{CH} components for the N and S hemispheres;

—Six-month components, i.e., monthly components of the corresponding values smoothed over half a year;

—The mean S_{CH} value level, i.e., the linear approximation of the monthly components for the detection of a rough S_{CH} trend in polar and isolated components.

Figure 1 shows the northern (black curve) and southern (gray curve) components of the monthly SNs smoothed over six months for the entire study period. It can be seen that the S hemisphere was dominant with respect to the sunspot number from the beginning of this period until March 2015, after which the sunspot activity shifted to the N hemisphere. This trend continued until the end of 2019, which is consistent with the results previously obtained by other authors: (http://sidc.oma.be/silso/monthlyhemisphericplot). The fact that there are two distinct periods in which the sunspot activity predominated in the declining phase is one of the features of cycle 24. Since we were interested in what happens with CHs in this phase of the cycle, we used this information to analyze S_{CH} variation over time.

3. TOTAL CORONAL HOLE AREAS

As a result of the processing of the array of CH areas extracted from the EUV images by the SPoCA, we obtained the temporal variations of the daily total CH area for the entire visible surface of the solar disk (Fig. 2a) and separately for both hemispheres (Figs. 2b and 2c). In all three panels of Fig. 2, the hollow squares are S_{CH} and the black curves are the monthly smoothed values of the corresponding components.

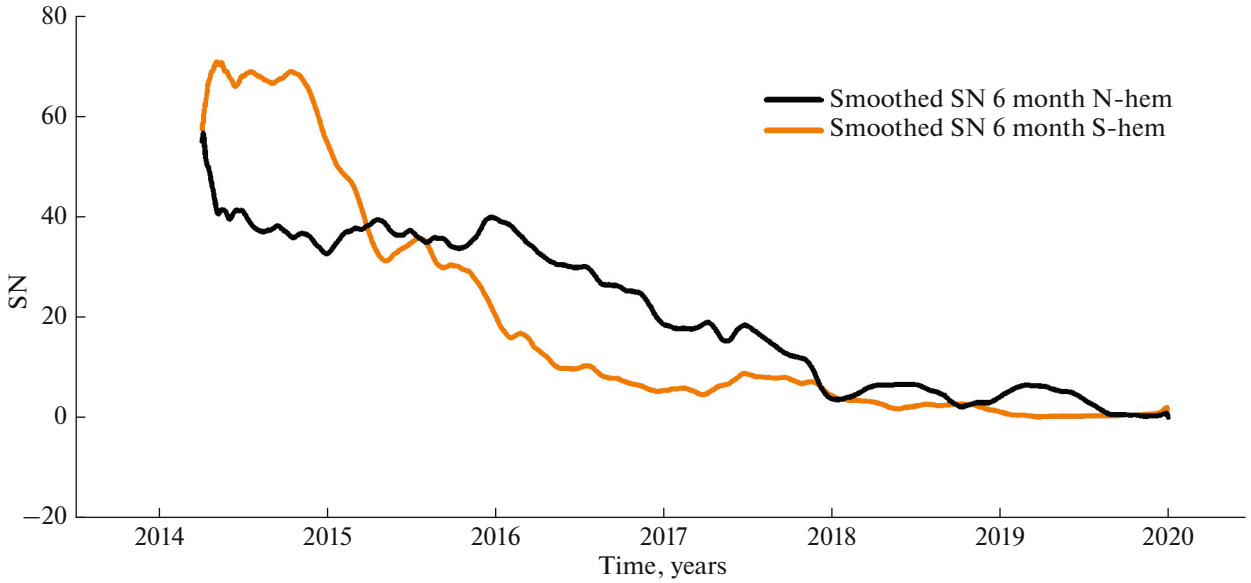

Fig. 1. Monthly SN components smoothed over half a year: northern (black line) and southern (orange line).

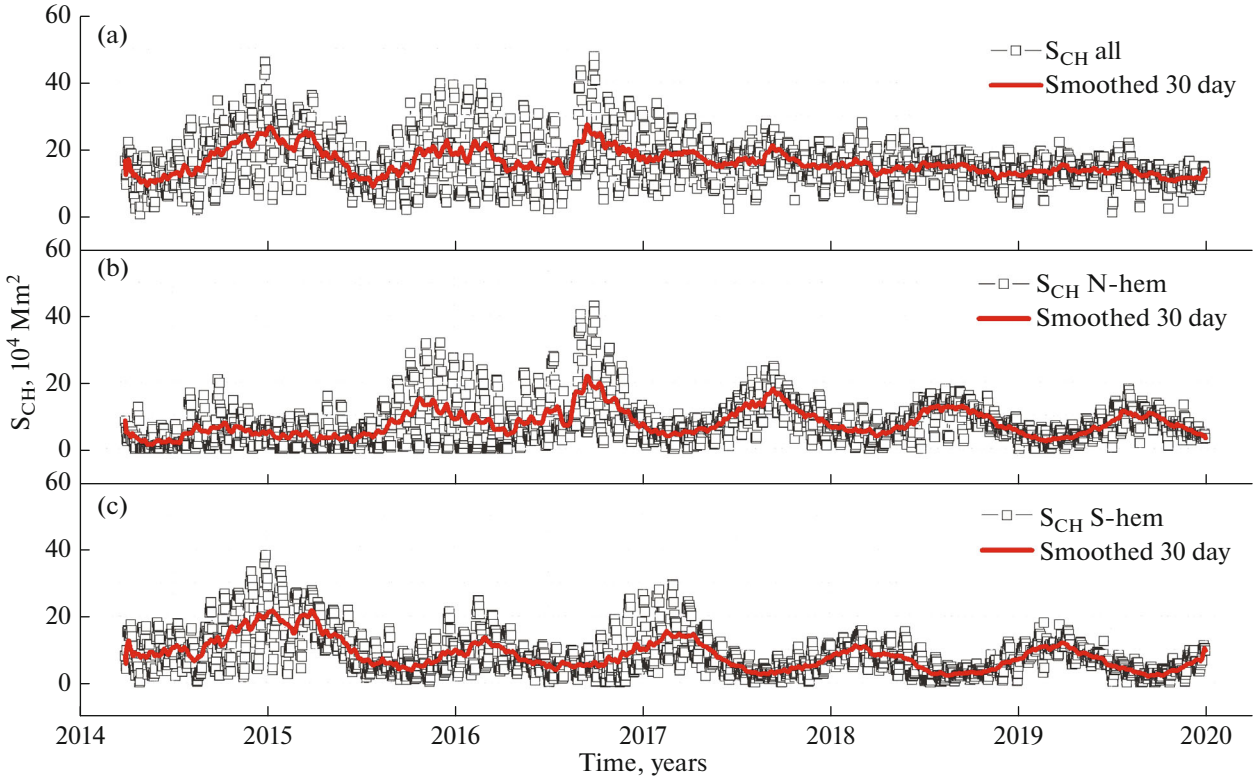

Fig. 2. Temporal variations of the daily total CH area on the branch of activity decline of cycle 24: (a) for the entire visible surface of the Sun, (b) for the N hemisphere, and (c) for the S hemisphere. The hollow squares are the S_{CH}, and the red curve is S_{CH} smoothed over a month.

The first stage of the study period (April 2014–March 2015) is marked by the dominance of the S hemisphere by S_{CH} (Fig. 2c). However, starting from September 2015, it is replaced by the N hemisphere, as in the case of SN but with a delay of about half a year (Fig. 2b). The fact that the sunspot activity at this stage anticipates the increase in CH areas was noted in our previous work (Andreeva et al., 2020).

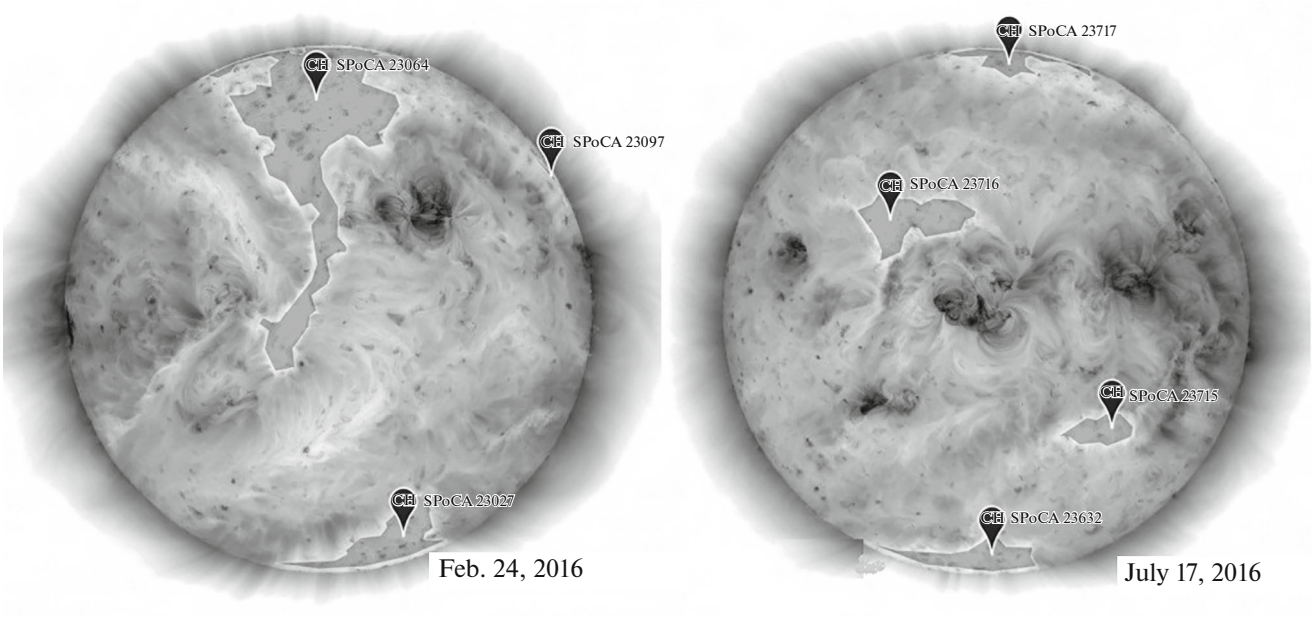

Fig. 3. Inverted images of the Sun obtained by the SDO/AIA on Feb. 24, 2016, and July 17, 2016, in the Fe XII line (19.3 nm). The areas on the solar disk marked with CH are CHs extracted from the EUV image with SPoCA. Coronal holes with SPoCA 23027, 23064, 23632, and 23717 are polar, and those with SPoCA 23097, 23715, and 23716 are isolated. Dark formations on the solar disk marked with AR are active regions.

From April 2014 to mid-2017, the S_{CH} amplitudes changed in a fairly wide range [0: 45×10^4 Mm^2]. After that, the S_{CH} amplitude range narrows by about two times. The noticeable increase in the CH area during this period is due to the reappearance of several giant CHs (GCHs), which remained for a series of solar rotations (SRs). One of them, the longest lasting GCH of the N hemisphere (Fig. 2b, June 2015–February 2017), was observed and studied in our work (Andreeva et al., 2018). During its evolution, the GCH occupied a significant part of the N hemisphere, ~ 8×10^{11} km^2. The GCH evolution included the passage of two active centers through it, which affected the change of many of its parameters. The GCH had a significant impact on the processes of the N hemisphere.

The visible, quasi-synchronous behavior of CHs in the N and S hemispheres in Figs. 2b and 2c and Figs. 5a and 5c reflects the change in the slope of the solar rotation axis during the year.

4. TEMPORAL CHANGES IN THE TOTAL POLAR AND ISOLATED CORONAL-HOLE AREAS

Sanchez-Ibarra and Barraza-Paredes (1992) divided all CHs into two classes, equatorial and polar, with respect to their topological relationship to the polar regions. A typical polar CH (CH_pol) appears as a CH spike in the polar region extending to the low latitude region. In turn, equatorial CHs are observed at low latitudes within the royal zone, where ARs develop, and are isolated islands that are not related to polar CHs. The term *equatorial holes* does not seem to be optimal, because this class formally includes high-latitude objects that are located away from the equator but are not related to polar holes. From this perspective, the terms *isolated* (Yazev, 2010) or *nonpolar* CHs are more appropriate (Bilenko and Tavastsherna, 2016). Insley et al. (1995) pointed out that these two classes of CHs are two populations that differ in their rotation patterns and developmental characteristics during the cycle.

Polar CHs usually disappear during the solar cycle maximum and appear again, already with a magnetic flux of opposite polarity, thus demonstrating a change in the polar field. Isolated CHs behave differently: they appear during the early phases of increase in solar activity, though usually more frequently at the maximum, and disappear near the activity minimum.

After the polarity reversal, the spikes of polar holes merge with the regions resulting from the evolution of the AR tails following the polarity rule. In the initial phase of the cycle decline, the situation seems favorable for the formation of large, isolated equatorial holes (Yazev, 2010; Abramenko et al., 2006, 2010), because bipolar magnetic regions at low latitudes from different hemispheres can form large, unipolar cells upon merging. Finally, there is no significant number of ARs at the cycle minimum. Therefore, there is no basis for the formation of regions capable of generating CHs over time. During this period, the magnetic flux

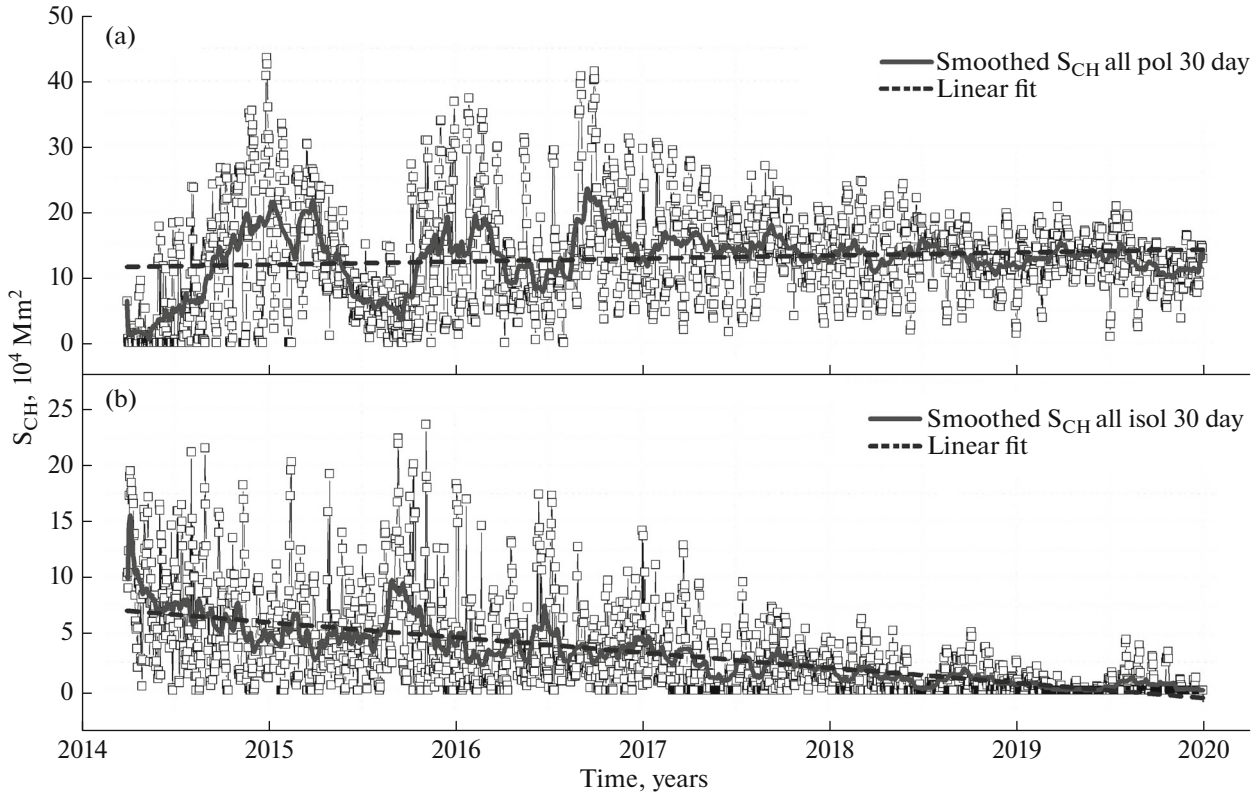

Fig. 4. Change in the daily total area (hollow squares) of all polar (a) and isolated (b) CHs on the visible surface of the solar disk in the period Apr. 1, 2014–Dec. 31, 2019. The solid black curves are the CH area smoothed over a month. The dashed lines are a linear approximation of the areas smoothed over a month, the mean levels of the total polar and isolated CH areas.

at the poles is maximal, and the polar regions are maximally developed (Yazev, 2010).

In this article, we studied two types of CHs, polar (CHs_pol) and isolated (CHs_isol). Figure 3 gives an example of such CHs. The first group is polar CHs, which are located at the solar poles (SPoCA 23064, 23027, 23717, 23632) and have a lifetime comparable to that of the solar cycle. Extensions of CHs, such as the *elephant trunk* (SPoCA 23064), also belong to this category. The second type is isolated or nonpolar CHs (SPoCA 23715, 23716, 23097), which are mostly limited to low, medium, and sometimes high latitudes, but not related to polar CHs. Their lifetime is comparable to several CRs.

Figs. 4a and 4b show the variations of the total polar and isolated CH areas for the entire visible surface of the solar disk, and they are shown separately for the N and S hemispheres in Fig. 5.

Against the background of the daily total polar (a) and isolated (b) CH areas (squares), Fig. 4, shows their values smoothed over a month and approximated (the black solid curve and dashed straight line, respectively) for the entire visible surface of the solar disk. The direction of the dotted line reflects the trend of the mean level of the total CH area during the considered period. It can be seen that it increases in this phase of the cycle for polar CHs (Fig. 4a) and decreases for isolated CHs (Fig. 4b). In the entire studied period, the mean level of the polar CH areas varied within $11.5 \times 10^4 < \text{Sum } S_{CH\_pol} < 14.5 \times 10^4$ Mm^2 and the isolated areas varied within $0 < \text{Sum SCH\_isol} < 7 \times 10^4$ Mm^2.

The maximum amplitudes of polar CH areas are observed at the beginning of the decline phase and seem to be related to the ongoing restructuring after the second maximum of cycle 24 and the presence of several GCHs between April 2014 and September 2017. The GCH was first observed in the S hemisphere (Fig. 5c, April 2014–April 2015), then in the N hemisphere (Fig. 5c, June 2015–January 2017), and then again in the S hemisphere (Fig. 5c, August 2016–June 2017). The spikes in the amplitudes of the polar-CH areas at these moments are clearly visible in Fig. 5a. The amplitudes of the isolated-CH areas also had the maximum values during this period, but they were significantly smaller than those for polar-CH areas. After June 2017, the mean level of the total polar-CH areas approached 14×10^4 Mm^2 (Fig. 4a). The situation stabilized, and the amplitude range of the polar-CH area significantly decreased.

It can be seen from Fig. 4 that the total polar-CH areas predominated during the studied stage. The

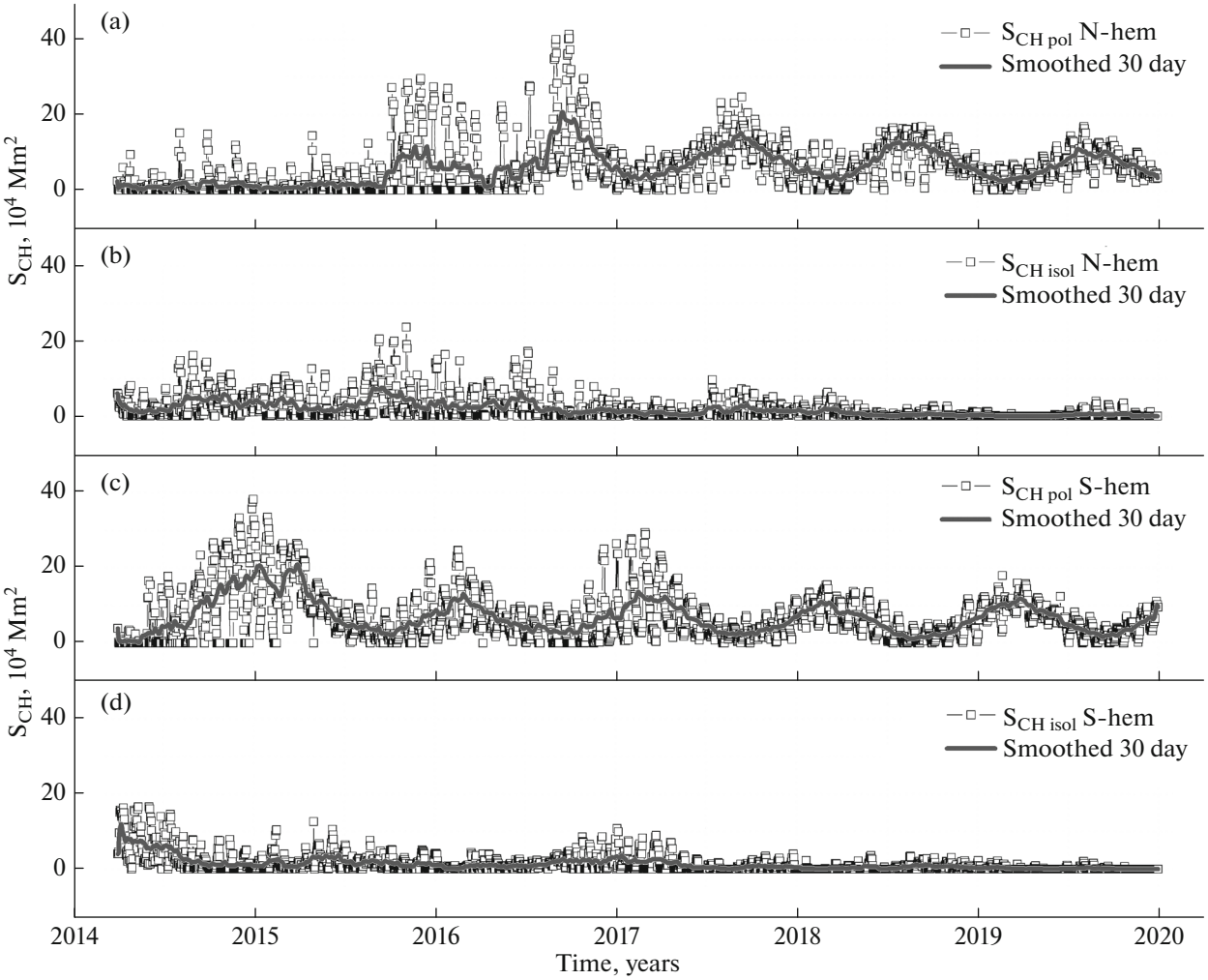

Fig. 5. Daily total areas of polar (a, c) and isolated (b, d) CHs of the N (a, b) and S (c, d) hemispheres. The black lines are the monthly smoothed components of the daily total CH area.

range of amplitude variation of the total daily polar-CH areas was 0–45 × 10^4 Mm^2, while it was only 0–23 × 10^4 Mm^2 for the isolated areas (squares in Figs. 4a and 4b). We determined the contribution of the areas of the two CH types to the total area for the studied period. It turned out that the total area of all CHs was 33508.53 × 10^4 Mm^2, 26873.93 × 10^4 Mm^2 of which were polar and 6669.43 × 10^4 Mm^2 were nonpolar. In percentage terms, it was ~80% and ~20%. With this in mind, our result is consistent with the conclusion drawn by Bravo and Stewart (1997) that the total area of all CHs becomes maximal toward cycle minimum.

The following can be noted upon analysis of the temporal distribution of polar- and isolated-CH areas across hemispheres (Fig. 5): at the beginning of the studied period, giant, recurrent polar CHs followed each other with some periodicity during the first 4 years (Figs. 5a and 5c). There were very strong increases and decreases in S_{CH_pol} (the black curve in Figs. 4a, 5a, and 5c). The situation stabilized after the middle of 2017, but the N hemisphere continued to predominate to a certain extent in terms of the area occupied by CHs.

5. CONCLUSIONS

The dynamics of CHs in the declining phase of cycle 24 was studied. Comparison of the variations in the daily total CHs areas with the index of sunspot number made it possible to reveal some features of the variation of the polar- and isolated-CHs areas in the period April 1, 2014–December 31, 2019.

During the studied period, there was an asymmetry in the distribution of S_{CH} and SN across hemispheres; the dominance of the S hemisphere changed to that of the N hemisphere.

The division of all CHs from the considered period into polar and nonpolar ones showed that polar-CH areas predominated and increased, while nonpolar-CH areas constantly decreased toward the cycle mini-

mum. The polar-CH areas accounted for ~80% of the total area of all considered CHs during the studied period.

The total area of polar CHs increases toward solar cycle minimum, which is consistent with the general concept of polar CHs as the main source of the Sun's dipole magnetic field (Ikhsanov and Ivanov, 1999; Webber et al., 2014). This conclusion is consistent with previous studies (Bravo and Stewart, 1997; Dorotovič, 1996). In this case, the second subset, isolated CHs, shows an interesting behavior in the declining phase of the solar activity that was not previously observed. Their areas slowly decrease from the maximum to the minimum of the solar cycle. This trend is qualitatively consistent with a decrease in sunspot activity toward the minimum, which suggests a physical relationship between the two phenomena. However, the latter conclusion requires further verification with data from other solar cycles. Regardless of the result of such verification, it is already clear that the open magnetic flux from the entire Sun is not uniform in composition.

It was noted that the visible quasi-synchronous behavior of polar CHs in the N and S hemispheres reflects the change in the tilt of the Sun's rotation axis during the year.

ACKNOWLEDGMENTS

The SDO is part of the Living with a Star program of the National Aeronautics and Space Administration. The SDO/AIA data were provided by the Joint Science Operation Center (JSOC). We thank the Heliophysics Event Knowledgebase (HEK) project team for access to the CH databases.

We are grateful to V.I. Abramenko for useful discussions, valuable suggestions, and critical comments.

We thank the anonymous reviewer whose comments and critiques made it possible to improve the article.

CONFLICT OF INTEREST

The authors declare that they have no conflict of interest.

REFERENCES

Abramenko, V.I., Fisk, L.A., and Yurchyshyn, V.B., The rate of emergence of magnetic dipoles in coronal holes and adjacent quiet-Sun regions, *Astrophys. J.*, 2006, vol. 641, no. 1, pp. L65–L68.

Abramenko, V., Yurchyshyn, V., Linker, J., et al., Low-latitude coronal holes at the minimum of the 23rd solar cycle, *Astrophys. J.*, 2010, vol. 712, no. 2, pp. 813–818.

Andreeva, O.A., Akhmetov, Z.S., Malashchuk, V.M., et al., Study of variations of some characteristics of the giant coronal hole of 2015–2017, *Geomagn. Aeron. (Engl. Transl.)*, 2018, vol. 58, no. 7, pp. 916–924.

Andreeva, O.A., Abramenko, V.I., and Malashchuk, V.M., Coronal holes during the period of maximum asymmetry in the 24th solar activity cycle, *Astrophysics*, 2020, vol. 63, no. 1, pp. 114–124.

Barra, V., Delouille, V., Kretzschmar, M., and Hochedez, J.-F., Fast and robust segmentation of solar EUV images: Algorithm and results for solar cycle 23, *Astron. Astrophys.*, 2009, vol. 505, no. 1, pp. 361–371.

Bilenko, I.A., Formation and evolution of different type coronal holes, in *Multi-Wavelength Investigations of Solar Activity, Proceedings IAU Symposium*, Stepanov, A.V., Benevolenskaya, E.E., and Kosovichev, A.G., Eds., 2004, vol. 223, pp. 373–374.

Bilenko, I.A. and Tavastsherna, K.S., Coronal hole and solar global magnetic field evolution in 1976–2012, *Sol. Phys.*, 2016, vol. 291, pp. 2329–2352.

Bohlin, J.D. and Sheeley, N.R., Jr., Extreme ultraviolet observations of coronal holes, *Sol. Phys.*, 1978, vol. 56, pp. 125–151.

Bravo, S. and Otaola, J.A., Polar coronal holes and the sunspot cycle: A new method to predict sunspot numbers, *Sol. Phys.*, 1989, vol. 122, pp. 335–343.

Bravo, S. and Stewart, G.A., Evolution of polar coronal holes and sunspots during cycles 21 and 22, *Sol. Phys.*, 1994, vol. 154, pp. 377–384.

Bravo, S. and Stewart, G.A., The correlation between sunspot and coronal hole cycles and a forecast of the maximum of sunspot cycle 23, *Sol. Phys.*, 1997, vol. 173, no. 1, pp. 193–198.

Dorotovič, I., Area of polar coronal holes and sunspot activity: Years 1939–1993, *Sol. Phys.*, 1996, vol. 167, pp. 419–426.

Hess Webber, S.A., Karna, N., Pesnell, W.D., and Kirk, M.S., Areas of polar coronal holes from 1996 through 2010, *Sol. Phys.*, 2014, vol. 289, pp. 4047–4067.

Hoyng, P., Helicity fluctuations in mean field theory: An explanation for the variability of the solar cycle?, *Astron. Astrophys.*, 1993, vol. 272, pp. 321–339.

Hurlburt, N., Cheung, M., Schrijver, C., et al., Heliophysics event knowledgebase for the Solar Dynamics Observatory (SDO) and beyond, *Sol. Phys.*, 2012, vol. 275, pp. 67–78.

Ikhsanov, R. and Ivanov, V., Properties of space and time distribution of solar coronal holes, *Sol. Phys.*, 1999, vol. 188, pp. 245–258.

Insley, J.E., Moore, V., and Harrison, R.A., The differential rotation of the corona as indicated by coronal holes, *Sol. Phys.*, 1995, vol. 160, no. 1, pp. 1–18.

Levine, R.H., Large-scale solar magnetic fields and coronal holes, in *CHs and High Speed Wind Streams*, Zirker, J.B., Ed., Boulder, Col.: Colorado Univ. Press, 1977, pp. 103–143.

Levine, R.H., Altschuler, M.D., Harvey, J.W., and Jackson, B.V., Open magnetic structures on the Sun, *Astrophys. J.*, 1977, vol. 215, pp. 636–651.

Malashchuk, V.M., Fainshtein, V.G., Stepanyan, N.N., and Rudenko, G.V., Connection of coronal holes with active regions, *Bull. Crimean Astrophys. Obs.*, 2012, vol. 108, no. 1, pp. 64–69.

Obridko, V.N. and Shelting, B.D., Global complexes of activity, *Astron. Rep.*, 2013, vol. 57, no. 10, pp. 786–796.

Obridko, V.N. and Shelting, B.D., Coronal holes in global complexes of activity, *Adv. Astron.*, 2015, vol. 2015, pp. 1–9.

Sanchez-Ibarra, A. and Barraza-Paredes, M., Catalog of coronal holes, 1970–1991, Report UAG-102, Boulder, Col.: World Data Center A for Solar-Terrestrial Physics, National Geophysical Data Center,1992.

Sheeley, N.R., Jr. and Harvey, J.W., Coronal holes, solar wind streams, and geomagnetic disturbances during 1978 and 1979, *J. High Resolut. Chromatogr. Chromatogr. Commun.*, 1981, vol. 70, pp. 237–249.

Verbeeck, C., Delouille, V., Mampaey, B., and De Visscher, R., The SPoCA-suite: Software for extraction, characterization, and tracking of active regions and coronal holes on EUV images, *Astron. Astrophys.*, 2014, vol. 561, id A29.

Yazev, S.A., Coronal holes and solar activity complexes, *Izv. Irkutsk. Gos. Univ.: Ser. Nauki Zemle*, 2010, vol. 3, no. 2, pp. 226–241.

Translated by O. Pismenov